ACS Energy LETTERS

http://pubs.acs.org/journal/aelccp

LETTER

Gradient-Doped Colloidal Quantum Dot Solids Enable Thermophotovoltaic Harvesting of Waste Heat

Amirreza Kiani,[†,⊥] Hamidreza Fayaz Movahed,[†,⊥] Sjoerd Hoogland,[†] Oleksandr Voznyy,[†] Remigiusz Wolowiec,[†] Larissa Levina,[†] F. Pelayo Garcia de Arquer,[†] Patrick Pietsch,[†,‡] Xihua Wang,[†,§] Pouya Maraghechi,[†] and Edward H. Sargent*[,†]

[†]Department of Electrical and Computer Engineering, University of Toronto, 10 King's College Road, Toronto, Ontario M5S 3G4, Canada

[‡]Department of Information Technology and Electronics, ETH Zürich, ETZ H67, Gloriastrasse 35, 8092 Zürich, Switzerland

[§]Department of Electrical and Computer Engineering, University of Alberta, Edmonton, Alberta T6G 2 V4, Canada

Supporting Information

ABSTRACT: **Electromagnetic radiation emitted from hot objects represents a sizable source of energy, one that in most applications is not harvested efficiently. Even for a blackbody at 800 °C, the radiation intensity peaks near 2.7 μm wavelength, and this requires a semiconductor absorber having a band gap in the short-wavelength infrared and beyond to enable thermophotovoltaic (TPV) heat recovery. Here we report the first solution-processed TPV device to harvest efficiently 800 °C heat. The active layer consists of colloidal quantum dots (CQDs), infrared-absorbing nanoparticles synthesized using a scalable solution-based method, having 0.75 eV band gap. We construct rectifying junction devices based on controllably p- and n-doped CQD solids that benefit from a gradient in electron affinity that extends over the devices' thickness. The gradient-doped architecture relies on engineered charge carrier drift and overcomes the existing limitations of small band gap CQD solids. The devices provide 2.7% efficiency in the conversion of optical power from above-band gap photons from a blackbody source at 800 ± 20 °C into electrical power. The cells were thermally stable up to 140 °C, increasing the promise of CQD solids for TPV applications.**

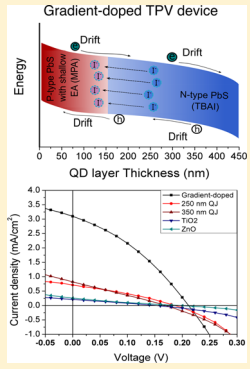

Subunity energy conversion efficiency in systems such as integrated circuits, solar cells, lasers, and internal combustion engines results in the generation of heat.[1] This heat is normally a wasted source of energy: if a portion of it were recycled back into electrical power, this could considerably increase the net performance of such systems.[2]

Thermophotovoltaic (TPV) devices are promising candidates to convert waste heat into electrical power. They utilize a small band gap semiconductor that absorbs the low-energy infrared photons from radiated thermal energy and use asymmetric contacts to the absorber to transfer net electrical power to a load.

Efforts to develop TPV devices date back more than 50 years: initial attempts used silicon as the absorbing semiconductor,[3] but the mismatch between the radiation spectra of the waste heat and the band gap of these semiconductors limited their use to the conversion of radiation from emitters having temperatures above 2000 °C.[4,5] This precluded effective recycling of most waste heat; as one example, for a blackbody emitter with a temperature of 1000 °C, the vast preponderance of radiated power resides in the infrared spectral region (99.64% of emitted power is greater than 1000 nm in wavelength).[6]

Significant advances were achieved using III−V compound semiconductors, such as gallium antimonide (GaSb) as TPV cells. Additionally, improved TPV design and spectral control techniques renewed the appeal in TPV devices.[7−9] Today, the best-performing TPV devices still rely on III−V compounds such as InGaAs or InGaAsSb.[10,11] For a blackbody emitter at 1050 °C, TPV devices based on InGaAs with a band gap of 0.6 eV (i.e., 2070 nm) can convert 19% of the above-band gap photon energy into electrical power.[12]

However, though their efficiencies are impressive, TPV devices based on ternary and quaternary alloys are costly and have therefore not yet achieved widespread deployment in energy recovery. The physical rigidity of these cells further limits their widespread use.

Received: August 1, 2016
Accepted: September 6, 2016
Published: September 6, 2016

DOI: 10.1021/acsenergylett.6b00314
ACS Energy Lett. 2016, 1, 740−746

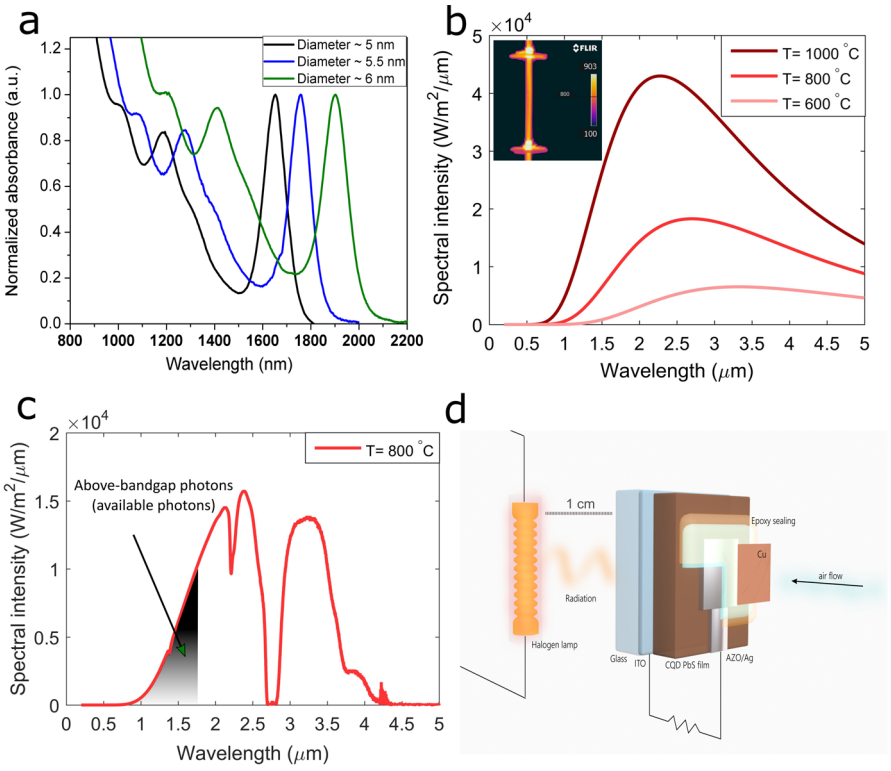

Figure 1. CQD-based TPV system. (a) Experimental solution absorption spectra of PbS CQDs with 5, 5.5, and 6 nm average diameter. Sharp peaks correspond to excitonic transitions between quantum confined levels. (b) Spectral radiation intensity for a blackbody source at 600, 800, or 1000 °C. As the blackbody temperature increases, the peak of radiation intensity shifts toward shorter wavelengths. The inset shows the lamp filament at 800 °C, measured using a thermal imaging camera with high accuracy. (c) Modified blackbody spectrum at 800 °C that takes into account the absorption of 1 mm fused silica (i.e., the fused silica bulb in the tungsten halogen lamp). The highlighted portion of the lamp corresponds to the photons with energy larger than the band gap of the PbS CQDs (available photons). (d) Schematic of the TPV setup. A tungsten-halogen lamp at 800 °C (blackbody emitter) was placed at a distance of 1 cm from the TPV cell. The TPV cell comprises a thick layer of CQDs on an ITO-coated glass substrate. Sputtered AZO and silver form the top contact. The device was then coated with an ultraviolet (UV)-cured epoxy and a heat-transfer epoxy. A copper plate was then placed on the epoxies to improve the heat transfer. The cell was cooled using airflow.

TPV cells that are both cost-effective and flexible, and could therefore be conformally coated to collect thermal energy radiated from hot emitters such as automobile exhaust pipes and industrial exhaust flues, could potentially render TPV practical for wider deployment.

Colloidal quantum dots (CQDs) are solution-processed nanoparticles that benefit from quantum size-effect tuning and that display facile band gap tunability via size control at the time of synthesis. This property, combined with the CQDs' inexpensive manufacturing processes and the wide variety of deposition techniques,[13,14] makes these materials promising candidates to serve as semiconductor absorbers for TPV cells. CQDs can be tuned well into the infrared (IR).[15] Their application in solar energy harvesting has recently risen to certified 11.3% power conversion efficiencies (PCE).[16−18] The IR energy-harvesting capability has also been successfully exploited for smaller band gap CQDs in tandem solar cells[19] and was recently investigated as a route to improve the performance of perovskite and silicon solar cells.[20]

In addition to requiring IR performance and band gap tunability, TPV applications also require cells to operate at and above 100 °C. This requires progress in the design of the CQD solid. Improving TPV performance overall demands further progress in extracting photocarriers from thick (>300 nm) light-absorbing layers.

Here we report the design and realization of solution-processed colloidal quantum dot solids as the active layers within TPV devices employing 0.75 eV band gap CQDs. The devices show stable behavior up to 140 °C and an absorbed-waste-heat-to-electrical-power conversion efficiency of 2.7% for the case of a blackbody emitter at 800 ± 20 °C. Thanks to the graded-doping architecture developed here, the thickness of the cell was increased for improved IR absorption while maintaining efficient charge extraction. As a result, we report stable performance under continuous operation at temperatures that exceed 100 °C.

We focused on a model system consisting of 0.75 eV band gap lead sulfide (PbS) CQD solutions (black spectrum in Figure 1a). We used a tungsten-halogen lamp as the blackbody emitter. The temperature of the filament was set to 800 °C as measured by fitting the partial spectral profile of the lamp with Planck's formula for blackbody emission. Furthermore, to improve the precision of the experiment, we measured the filament temperature directly using a thermal imaging camera with an accuracy of ±2% (Figure 1b inset). Blackbody emission spectra calculated using Planck's formula for objects at different temperatures are shown in Figure 1b. The tungsten filament is encapsulated by 1 mm thick fused silica, which modifies the full emission spectrum. Figure 1c shows the blackbody emission spectrum at 800 °C that takes into account the fused silica absorption profile. The highlighted part of the emission

DOI: 10.1021/acsenergylett.6b00314
ACS Energy Lett. 2016, 1, 740−746

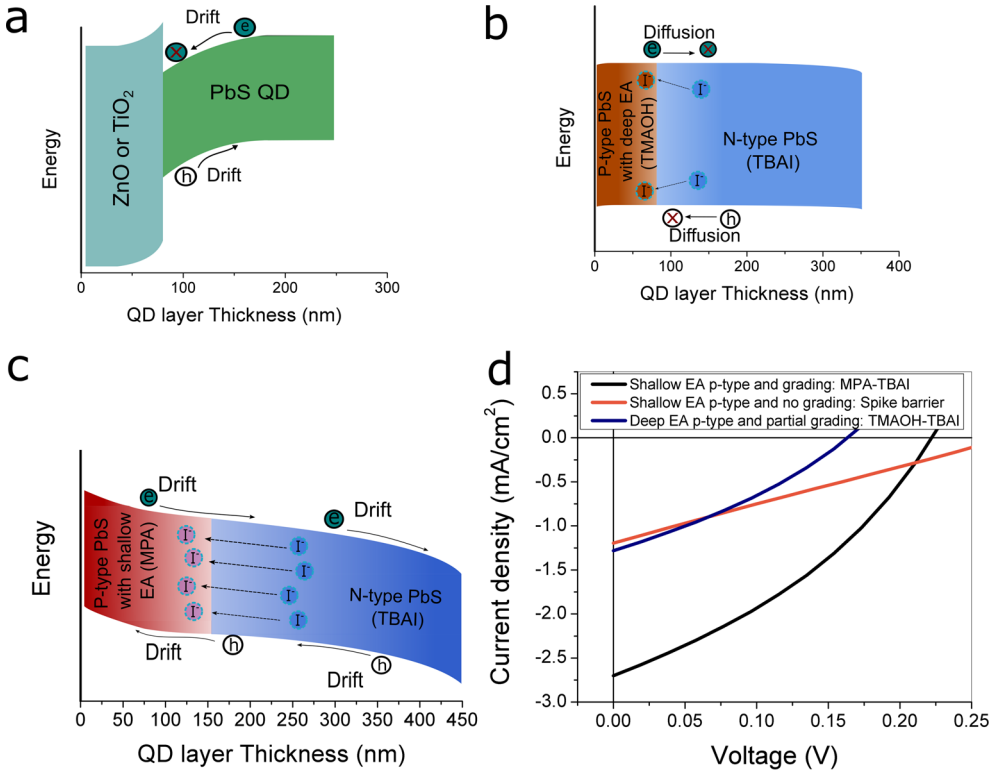

Figure 2. TPV device architectures and their operation. (a) Misalignment of the band structure between small band gap PbS CQDs (e.g., 0.75 eV dots used in this study) and ZnO or TiO_2 transparent conductive oxides. (b) P-type PbS CQDs with deep EA (e.g., TMAOH) cannot provide sufficient EA offset for a gradient architecture over a thick device. Hence, charge extraction will be limited and determined by charge carrier diffusion. Device thickness in this architecture cannot be increased without a detrimental effect on performance. Also, a barrier for hole injection into the electrode (i.e., ITO) can form because of the deep EA of the p-type layer. (c) Gradient-doped architecture developed in this study. MPA-treated PbS QDs provide the shallow EA of the p-type layer, while iodide diffusion brings a smooth change in doping and EA throughout the structure. The device thickness can be increased substantially to an optimized 450 nm as the charge collection depends less on diffusion in the presence of a built-in electric field. (d) One-dimesional optoelectronic device modeling reveals that the p-type layer with shallow EA (e.g., MPA) and gradient in EA are both required simultaneously for substantial improvement in device performance and to avoid formation of an undesired energy spike barrier.

spectrum corresponds to the available photons, which have energy larger than the band gap of the CQDs and thus can be absorbed and converted into electrical current. Using the 0.75 eV band gap CQDs we then fabricated TPV devices. In our test setup, shown in Figure 1d, we placed our TPV cells at a distance of 1 cm from the tungsten-halogen lamp. The TPV cells were coated with epoxy to protect the cells against oxidation and to facilitate cooling of the cell.

Photovoltaic device operation requires the efficient transfer of photogenerated carriers throughout the active layer, followed by their collection at the electrodes. Zinc oxide (ZnO) and titanium dioxide (TiO_2) have been studied extensively as electron acceptors for solar energy harvesting using PbS CQDs with a band gap of 1.3 eV. We found, however, that decreasing the CQD band gap below 0.8 eV, required for efficient TPV operation, led to a failure in electron injection into ZnO or TiO_2 due to band misalignment (Figure 2a).[21]

We therefore investigated the use of the quantum junction (QJ) architecture to provide improved control over the electron affinity (EA) offset between the different layers and avoid the use of selective contacts.[22] The QJ is a homojunction comprising a p-type and an n-type PbS CQD layer. We began by using tetramethylammonium hydroxide (TMAOH)- and tetrabutylammonium iodide (TBAI)-treated CQDs as the p- and n-type layers, respectively (Figure 2b).[23,24] However, we found experimentally that, in this case, the device thickness could not be increased over 250 nm without sacrificing the performance, suggesting poor carrier extraction over this active layer thickness. We proposed that, at this early stage of development, films based on 0.75 eV band gap CQDs have a high trap state density that limits collection length.[25,26]

We therefore pursued a device architecture that would overcome the need for extended photocarrier diffusion. We sought to implement a gradient in the electron affinity within the active CQD layer with the goal of producing a built-in electric field extended over the entire active layer thickness, shifting charge collection from diffusion to drift (Figure 2c).

Given the deep electron affinity (EA) of TBAI-treated CQDs,[27] a graded EA over a thick active layer would require a complementary shallow CQD p-type layer; however, the electron affinity of TMAOH-treated dots is not sufficiently shallow for this purpose. Furthermore, a p-type layer with deep EA (e.g., TMAOH) forms a less favorable junction with the hole-extracting contact (i.e., ITO in this study) compared to a shallower p-type layer, which can affect the device performance significantly (Figure 2b,c and Figure S1).

When a shallow p-type layer is used in combination with a deeper n-type layer, an undesired carrier-blocking energy spike can form at the interface, which will impede carrier extraction. The energy spike can be avoided via gradient in EA. One-dimensional (1D) optoelectronic device modeling (Figure 2d) shows that a sufficiently large EA offset and a gradient in

DOI: 10.1021/acsenergylett.6b00314
ACS Energy Lett. 2016, 1, 740−746

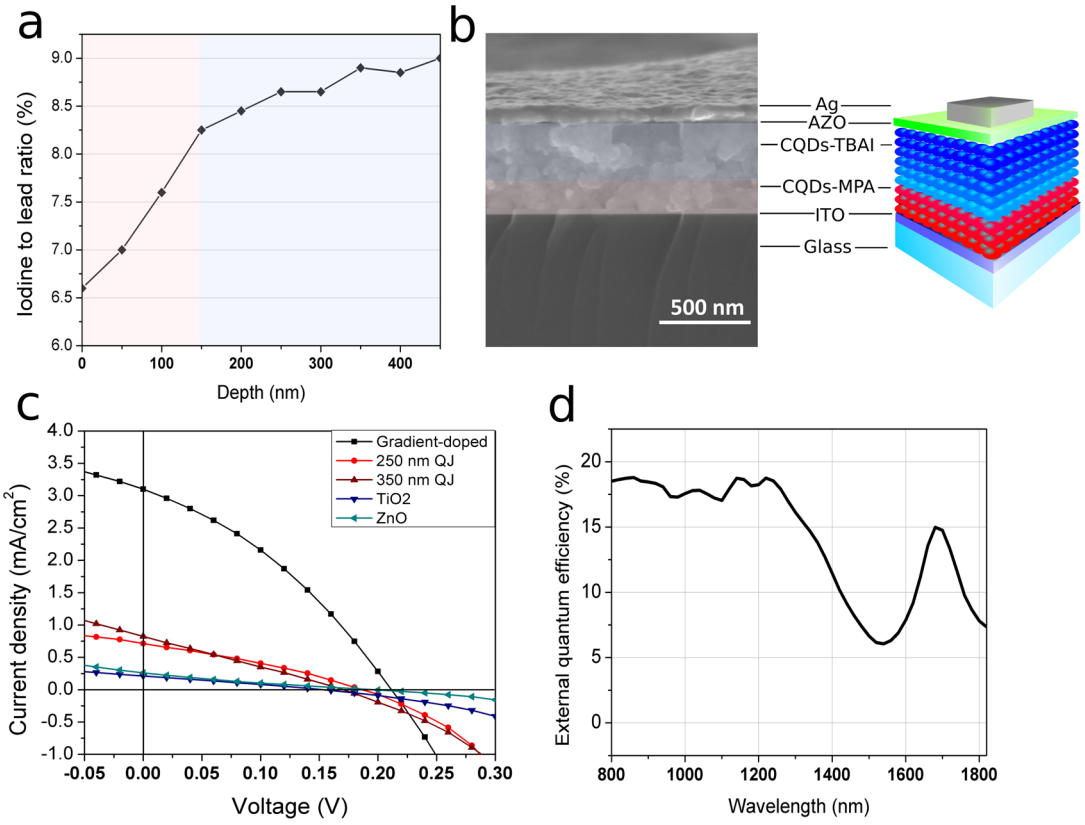

e

	J_{sc}(mA cm^{-2})	V_{oc} (V)	FF (%)	Available PCE (%)
Quantum junction TMAOH-TBAI (250 nm)	0.7	0.19	35	0.61 ± 0.04
Quantum junction TMAOH-TBAI (350 nm)	0.8	0.17	26	0.46 ± 0.03
Gradiant-doped device MPA-TBAI (450 nm)	3.1	0.21	32	2.70± 0.15

Figure 3. Gradient-doped TPV device characterization. (a) Sputtering XPS reveals that iodide can diffuse in the p-type layer and that the I:Pb ratio is graded throughout the device thickness. (b) Cross-sectional SEM image of the gradient-doped TPV device. The CQDs were deposited on the ITO-coated glass substrate. Sputtered AZO and evaporated silver formed the electron accepting layers. (c) Current density−voltage characterization of the TPV cells with different architectures. ZnO and TiO_2 based cells showed poor performance due to band misalignment. The performance of QJ devices based on TMAOH-TBAI dots was limited because of a large number of trap states. Increasing the active layer thickness by 100 nm resulted in lower V_{oc} and FF due to higher recombination. Gradient-doped TPV cell based on MPA-TBAI treated dots showed improved J_{sc}, V_{oc}, and FF. The thickness of the gradient-doped TPV cell was 450 nm. (d) External quantum efficiency spectrum of the gradient-doped TPV cell. (e) Details of thermophotovoltaic performance for different architectures. The PCE was calculated based on the available incident power of 7.6 ± 0.3 mW/cm^2 corresponding to the above band gap photons. The reported variation in the PCE is due to the variation of the power measurement (±0.3 mW/cm^2).

doping (i.e., EA) are both required simultaneously to achieve a substantial improvement in device performance and to avoid an energy spike barrier. Given the EA of mercaptopropionic acid (MPA), which is shallower than that for TMAOH-treated dots, we reasoned that this would be an ideal p-type layer candidate in the presence of the n-type TBAI layer, Figure S1.[27]

Additionally, a high mobility for iodide anions within CQD films provides the means to fabricate the desired graded EA. Sputtering X-ray photoelectron spectroscopy (XPS) (Figure 3a) confirmed that iodide can diffuse over long distances (hundreds of nm) and thus provide a gradient in iodine concentration. Hence, if deposited atop of the MPA p-type layer, a desired gradient in electron affinity and doping throughout the CQD film could be achieved. The spatial extent of the gradient could be controlled by changing the thickness of the bottom p-type layer.

A gradient TPV device schematic and its corresponding cross-sectional scanning electron microscope (SEM) image are shown in Figure 3b. The built-in electric field due to the graded EA allowed us to increase the active layer thickness to 450 nm, a substantial increase over the optimized 250 nm for the TMAOH-TBAI QJ devices. Figure 3c shows $J-V$ curves for different architectures explored in this study. For standard QJ devices, increasing the film thickness from 250 to 350 nm does not improve the performance. Because carrier diffusion plays a major role in the standard architecture, a thicker active layer results in increased carrier recombination and a lower open-circuit voltage (V_{oc}) and fill factor (FF). In contrast, the gradient-doped architecture shows significant improvements in all figures of merit (short-circuit current density (J_{sc}), V_{oc}, and FF) with increased active layer thickness, up to 450 nm.

Details of thermophotovoltaic performance are presented in Figure 3e. The tungsten-halogen blackbody emitter was set to

DOI: 10.1021/acsenergylett.6b00314
ACS Energy Lett. 2016, 1, 740−746

800 ± 20 °C, producing an incident radiation power density of 52.0 ± 2.0 mW/cm^2. This corresponds to an available above-band gap power density of 7.6 ± 0.3 mW/cm^2, calculated using the above-band gap photons (E_{ph} > 0.7 eV) (Experimental Methods). Considering the above-band gap photons, the best gradient-doped TPV cells delivered an efficiency of 2.7 ± 0.15% (available PCE). This performance is significantly higher (>4×) than that achieved using other architectures investigated in this study, Figure 3c,e.

Figure 3d shows the external quantum efficiency (EQE) spectrum of the gradient-doped TPV cell. The TPV device exhibits a prominent EQE at the exciton peak that rises up to 15% at 1700 nm. This indicates the successful extraction of carriers generated by low-energy photons, an achievement enabled by the graded doping and EA, and showcases the promise of CQDs in TPV applications.

We then sought to evaluate the thermal stability of the gradient-doped TPV cells, a crucial figure of merit for these devices. During the course of an initial 20-cycle study at 100 °C, graded cells displayed excellent stability, retaining their performance within 10% of the initial value (Figure 4a). We further explored the limit of thermal exposure for the graded TPV cells and found that the performance can be maintained up to 140 °C (Figure 4b).

In summary, this work reports the deployment of 0.75 eV PbS CQDs as the absorber in a thermophotovoltaic device designed for use with an 800 °C blackbody emitter. The gradient-doped architecture developed herein used p-type MPA-treated dots coupled to shallow EA and deeper TBAI-treated n-type dots. Sputtering XPS confirmed the diffusion of the iodide throughout the p-type layers that led to a smooth gradient in doping and EA that extends the collection length of the free carriers. The new graded architecture allowed a significant increase in the device thickness, as a result of which the cell delivered a promising 2.7% PCE (PCE referenced to above-band gap incident power). The gradient-doped cell showed good performance stability up to 140 °C.

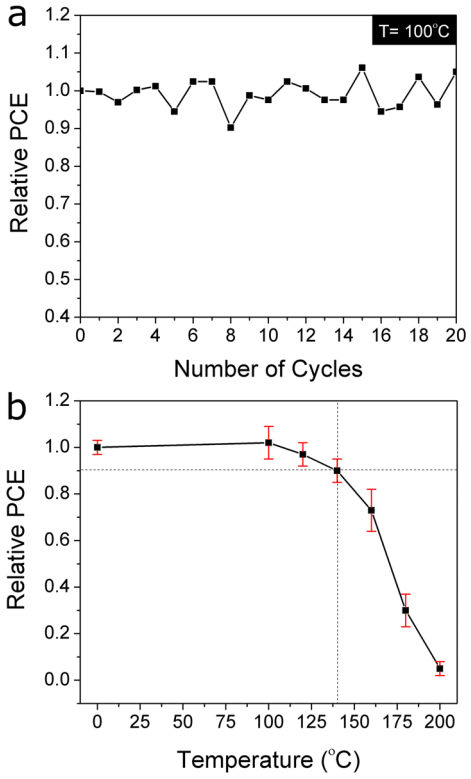

Figure 4. Evaluation of thermal stability. (a) Relative power output of the device, studied as a function of thermal cycling. (b) Relative power output of the same device studied as a function of annealing temperature. The device starts to fail at temperatures higher than 140 °C. The error bars are based on the standard deviation.

The PCE of 2.7% for the gradient-doped CQD-based TPV cells studied herein, for the case of an emitter temperature of 800 °C, represents an appreciable advance for solution-processed thermophotovoltaics. Future developments in CQD-based TPV devices will rely on improved synthesis of well-passivated small band gap CQDs as the field approaches the optimal band gap matched to TPV-relevant hot objects. The realization of thicker and well-passivated CQD films will result in a more efficient harvesting of the blackbody radiation spectrum. This will also benefit from photon management strategies that enhance infrared light trapping. Elimination of less stable organic ligands is also required for improved device stability and performance. TBAI-based devices are known to be more stable than MPA-based devices at both room and elevated temperatures.[24,28]

EXPERIMENTAL METHODS

Quantum Dot Synthesis and Thermophotovoltaic Device Fabrication. Colloidal quantum dots were prepared following the recipe previously reported by Hines and Scholes with some modifications.[29] At first, 1.8 g of lead oxide, 6.0 mL of oleic acid, and 27 mL of 1-octadecene were loaded in 250 mL round-bottom 3-neck flask. Then, the mixture was pumped at 100 °C for 60 min. After the solution turned optically clear, the temperature was set to the reaction temperature, which ranges from 140 to 155 °C. TMS solution in ODE (200 μL in 8 mL of ODE) was rapidly injected into reaction flask. The heating mantle was turned off but was not removed to provide slow cooling. The CQDs were isolated by addition of 25 mL of acetone and redispersed in anhydrous toluene. For the gradient-doped devices, colloidal quantum dot films were prepared by multilayer spin-casting of 40 mg/mL solution of PbS nanoparticles in a 3:1 mixture of octane:decane under ambient conditions. Each layer formed by depositing two drops of PbS solution (approximately 50 μL) on ITO-coated glass substrate at 2500 rpm. The layer was then soaked for 3 s in 10% 3-mercaptopropionic acid (MPA) in methanol followed by spinning at 2500 rpm. It was then rinsed with methanol while spinning at 2500 rpm to remove the excess oleic acid. For the n-type layer, the same procedure was applied, but instead tetrabutylammonium iodide (TBAI) was used for the ligand-exchange process. Each layer was soaked for 5 s in TBAI containing methanol solution. The TBAI concentration used in this study is 10 mg/mL. The device was then transferred into a glovebox with inert N_2 environment and left overnight. The ohmic contacts were the ITO substrate for the MPA-treated p-type quantum dots and sputtered aluminum doped ZnO (AZO) for the n-type quantum dots. Finally, an 80 nm thick silver contact was deposited by thermal evaporation at a rate of 0.4 Å/s at a pressure of <1 × 10^{-6} mbar. Contact size was 0.1667 cm^2. For the heterojunction devices, ZnO was prepared using a sol−gel technique. The 300 mM samples of zinc acetate dehydrate and ethanolamine were dissolved in 2-methoxyethanol solution and deposited on the ITO coated glass substrate at 3000 rpm to yield a 30 nm thick layer. The layer was annealed

DOI: 10.1021/acsenergylett.6b00314
ACS Energy Lett. 2016, 1, 740−746

at 175 °C for 10 min. The TiO_2 nanoparticles were synthesized using a previously published method.[20] MPA was used for the solid-state ligand exchange process, and 20 nm evaporated molybdenum trioxide and 50 nm thermally evaporated silver were used as the top contact at similar rate and pressure mentioned before. The QJ devices based on TMAOH as the p-type layer were made in the same manner as gradient-doped devices. The TMAOH solution consists of 0.75 mL of TMAOH in 10 mL of methanol. The CQD layer was soaked for 10 s in the TMAOH-containing solution before spinning at 2500 rpm for 10 s. The TMAOH treatment was followed by two washes with methanol to remove the excess oleic acid.

Blackbody Source. A linear tungsten-halogen lamp from Philips was used as the blackbody source. The blackbody was set to a temperature of 800 °C, as determined by fitting partial spectral profile of the emission with Planck's formula. Furthermore, the filament temperature was directly measured using a Flir T620 thermal imaging camera. The camera covers the temperature range of −40 to 2000 °C with the accuracy of ±2% of the reading temperature. The 1 mm fused silica absorption profile was taken from Thorlabs that accounts for the lamp's fused silica bulb. The absorption profile was used to calculate the modified blackbody spectrum. The blackbody source was placed at approximately 1 cm from the TPV cell. The radiation power density received by the cell was measured to be 52 ± 2 mW/cm^2 using a Melles Griot power meter through a circular 0.1667 cm^2 aperture at the position of the sample. The power meter is responsive from 200 nm to 20 μm. The accuracy of the power measurements was estimated to be ±5%

Thermophotovoltaic Performance Characterization. Current−voltage data was measured using a Keithley 2400 source meter after encapsulating the cell with UV-cured epoxy (Norland Optical adhesive 81). The cell was then coated with Arctic Silver's Arctic Alumina heat-transfer putty. A copper plate was placed on the top of the epoxies for an optimum heat transfer. The available power density of 7.6 ± 0.3 mW/cm^2 was obtained by integrating the modified blackbody spectral profile (Figure 1c) from 200 to 1775 nm considering the CQDs' practical optical band gap of 0.7 eV and a total measured power of 52 ± 2 mW/cm^2. The available power density was used to calculate the available PCE, Figure 3e.

Thermal Stability Measurement. The ramp rate is 0−100 °C in 1 min. The cells were kept at 100 °C for 10 min and then cooled for 5 min. After each thermal cycling the device performance was measured. The thermal cycling was repeated 20 times, and the cells showed stable performance with less than 10% fluctuation.

Sputtering XPS. XPS measurements were performed on a Thermo Scientific K-Alpha instrument using a 300 μm spot size and 50 eV pass energy. Sputtering was performed with argon ions at 2000 eV energy and "High" current setting for 30 s per level. The amount of iodine was normalized to total Pb signal at each sputtering level independently.

Scanning Electron Microscopy. Scanning electron microscopy (SEM) imaging was performed using an FEI Quanta Environmental SEM at a pressure of 6.3 × 10^{-4} Pa and operating voltage of 10 kV. The image was obtained using a secondary electron detector. Working distance was set to 10 mm.

EQE Measurements. External quantum efficiency spectrum was obtained by passing the output of a 450 W Xe lamp through a monochromator and using appropriate order-sorting filters. Calibrated Newport 818-UV and Newport 818-IR power meters were used to measure the collimated output of the monochromator through a 1 mm aperture. The measurement bandwidth was ∼40 nm, and the intensity varied with the spectrum of the Xe lamp. The current−voltage response was measured with Keithley 2400 source meters. Error in EQE measurements is estimated to be less than 5%.

Optoelectronic Modeling Details. Optoelectronic device modeling was performed using SCAPS software.[30] The absorption spectra of layers were based on measured ∼1650 nm CQD film absorption, and the electronic band gap was assumed to be 0.7 eV to account for bandtails. Doping densities of p-layer below 1016 cm^{-3} were used to account for the postsoaking by TBAI, while n-layer doping density of 1016 cm^{-3} was used. We used the 2 × 10^{-3} cm^2/(V s) electron and hole mobility in both layers. A linear gradient in EA and carrier density is implemented in the active layer. The thickness was assumed to be 120 nm for p-layer and 330 nm for n-layer. A trap density of 5 × 10^{-16} cm^{-3} with a trap depth of 0.3 eV below EC was used. Relative dielectric permittivity was approximated to be around 20 based on Maxwell−Garnet effective medium theory. Electron affinities of 4.1 eV for MPA, 4.4 eV for TMAOH, 4.5 eV for TBAI layers, and 4.1 eV for AZO and 4.8 eV for ITO electrodes were used.

■ ASSOCIATED CONTENT

Supporting Information

The Supporting Information is available free of charge on the ACS Publications website at DOI: 10.1021/acsenergylett.6b00314.

Density functional theory simulation showing the effect of different ligands on the EA of the PbS CQDs (PDF)

■ AUTHOR INFORMATION

Corresponding Author

*E-mail: ted.sargent@utoronto.ca.

Author Contributions

⊥A.K. and H.F.M. contributed equally to this work.

Notes

The authors declare no competing financial interest.

■ ACKNOWLEDGMENTS

The authors acknowledge funding from Total S.A. (grant no. 490037). The authors acknowledge the scientific and technical guidance of P. Sonntag, B. Voillequin, S. Roger, B. Swoboda, F. Geffray, A. Barriere, E. Palmiano, and D. Kopilovic.

■ REFERENCES

(1) Armstead, J. R.; Miers, S. A. Review of Waste Heat Recovery Mechanisms for Internal Combustion Engines. *J. Therm. Sci. Eng. Appl.* **2014**, *6*, 014001.

(2) Coutts, T. J. An Overview of Thermophotovoltaic Generation of Electricity. *Sol. Energy Mater. Sol. Cells* **2001**, *66*, 443−452.

(3) Broman, L. Thermophotovoltaics Bibliography. *Prog. Photovoltaics* **1995**, *3*, 65−74.

(4) Harder, N.-P.; Würfel, P. Theoretical Limits of Thermophotovoltaic Solar Energy Conversion. *Semicond. Sci. Technol.* **2003**, *18*, S151−S157.

(5) Van den Broeck, C. Thermodynamic Efficiency at Maximum Power. *Phys. Rev. Lett.* **2005**, *95*, 190602.

(6) Planck, M. *The Theory of Heat Radiation*; P. Blakiston's Son & Co: Philadelphia, 1914.

DOI: 10.1021/acsenergylett.6b00314
ACS Energy Lett. 2016, 1, 740−746

(7) Coutts, T. J.; Guazzoni, G.; Luther, J. An Overview of the Fifth Conference on Thermophotovoltaic Generation of Electricity. *Semicond. Sci. Technol.* **2003**, *18*, S144−S150.
(8) Bermel, P.; Ghebrebrhan, M.; Chan, W.; Yeng, Y. X.; Araghchini, M.; Hamam, R.; Marton, C. H.; Jensen, K. F.; Soljačić, M.; Joannopoulos, J. D.; et al. Design and Global Optimization of High-Efficiency Thermophotovoltaic Systems. *Opt. Express* **2010**, *18*, A314−A334.
(9) Chou, J. B.; Yeng, Y. X.; Lenert, A.; Rinnerbauer, V.; Celanovic, I.; Soljačić, M.; Wang, E. N.; Kim, S.-G. Design of Wide-Angle Selective Absorbers/emitters with Dielectric Filled Metallic Photonic Crystals for Energy Applications. *Opt. Express* **2014**, *22*, A144−A154.
(10) Dashiell, M. W.; Beausang, J. F.; Ehsani, H.; Nichols, G. J.; Depoy, D. M.; Danielson, L. R.; Talamo, P.; Rahner, K. D.; Brown, E. J.; Burger, S. R.; et al. Quaternary InGaAsSb Thermophotovoltaic Diodes. *IEEE Trans. Electron Devices* **2006**, *53*, 2879−2891.
(11) DeMeo, D.; Shemelya, C.; Downs, C.; Licht, A.; Magden, E. S.; Rotter, T.; Dhital, C.; Wilson, S.; Balakrishnan, G.; Vandervelde, T. E. GaSb Thermophotovoltaic Cells Grown on GaAs Substrate Using the Interfacial Misfit Array Method. *J. Electron. Mater.* **2014**, *43*, 902−908.
(12) Tan, M.; Ji, L.; Wu, Y.; Dai, P.; Wang, Q.; Li, K.; Yu, T.; Yu, Y.; Lu, S.; Yang, H. Investigation of InGaAs Thermophotovoltaic Cells under Blackbody Radiation. *Appl. Phys. Express* **2014**, *7*, 096601.
(13) Sargent, E. H. Infrared Photovoltaics Made by Solution Processing. *Nat. Photonics* **2009**, *3*, 325−331.
(14) Kramer, I. J.; Moreno-Bautista, G.; Minor, J. C.; Kopilovic, D.; Sargent, E. H. Colloidal Quantum Dot Solar Cells on Curved and Flexible Substrates. *Appl. Phys. Lett.* **2014**, *105*, 163902.
(15) McDonald, S. A.; Konstantatos, G.; Zhang, S.; Cyr, P. W.; Klem, E. J. D.; Levina, L.; Sargent, E. H. Solution-Processed PbS Quantum Dot Infrared Photodetectors and Photovoltaics. *Nat. Mater.* **2005**, *4*, 138−142.
(16) Lan, X.; Voznyy, O.; Kiani, A.; García de Arquer, F. P.; Abbas, A. S.; Kim, G.-H.; Liu, M.; Yang, Z.; Walters, G.; Xu, J.; et al. Passivation Using Molecular Halides Increases Quantum Dot Solar Cell Performance. *Adv. Mater.* **2016**, *28*, 299−304.
(17) Ning, Z.; Voznyy, O.; Pan, J.; Hoogland, S.; Adinolfi, V.; Xu, J.; Li, M.; Kirmani, A. R.; Sun, J.-P.; Minor, J.; et al. Air-Stable N-Type Colloidal Quantum Dot Solids. *Nat. Mater.* **2014**, *13*, 822−828.
(18) Yuan, M.; Liu, M.; Sargent, E. H. Colloidal Quantum Dot Solids for Solution-Processed Solar Cells. *Nat. Energy* **2016**, *1*, 16016.
(19) Wang, X.; Koleilat, G. I.; Tang, J.; Liu, H.; Kramer, I. J.; Debnath, R.; Brzozowski, L.; Barkhouse, D. A. R.; Levina, L.; Hoogland, S.; et al. Tandem Colloidal Quantum Dot Solar Cells Employing a Graded Recombination Layer. *Nat. Photonics* **2011**, *5*, 480−484.
(20) Ip, A. H.; Kiani, A.; Kramer, I. J.; Voznyy, O.; Movahed, H. F.; Levina, L.; Adachi, M. M.; Hoogland, S.; Sargent, E. H. Infrared Colloidal Quantum Dot Photovoltaics via Coupling Enhancement and Agglomeration Suppression. *ACS Nano* **2015**, *9*, 8833−8842.
(21) Kramer, I. J.; Sargent, E. H. The Architecture of Colloidal Quantum Dot Solar Cells: Materials to Devices. *Chem. Rev.* **2014**, *114*, 863−882.
(22) Tang, J.; Liu, H.; Zhitomirsky, D.; Hoogland, S.; Wang, X.; Furukawa, M.; Levina, L.; Sargent, E. H. Quantum Junction Solar Cells. *Nano Lett.* **2012**, *12*, 4889−4894.
(23) Ning, Z.; Ren, Y.; Hoogland, S.; Voznyy, O.; Levina, L.; Stadler, P.; Lan, X.; Zhitomirsky, D.; Sargent, E. H. All-Inorganic Colloidal Quantum Dot Photovoltaics Employing Solution-Phase Halide Passivation. *Adv. Mater.* **2012**, *24*, 6295−6299.
(24) Chuang, C.-H. M.; Brown, P. R.; Bulović, V.; Bawendi, M. G. Improved Performance and Stability in Quantum Dot Solar Cells through Band Alignment Engineering. *Nat. Mater.* **2014**, *13*, 796−801.
(25) Koh, W.; Saudari, S. R.; Fafarman, A. T.; Kagan, C. R.; Murray, C. B. Thiocyanate-Capped PbS Nanocubes: Ambipolar Transport Enables Quantum Dot Based Circuits on a Flexible Substrate. *Nano Lett.* **2011**, *11*, 4764−4767.
(26) Zhang, J.; Tolentino, J.; Smith, E. R.; Zhang, J.; Beard, M. C.; Nozik, A. J.; Law, M.; Johnson, J. C. Carrier Transport in PbS and PbSe QD Films Measured by Photoluminescence Quenching. *J. Phys. Chem. C* **2014**, *118*, 16228−16235.
(27) Brown, P. R.; Kim, D.; Lunt, R. R.; Zhao, N.; Bawendi, M. G.; Grossman, J. C.; Bulović, V. Energy Level Modification in Lead Sulfide Quantum Dot Thin Films through Ligand Exchange. *ACS Nano* **2014**, *8*, 5863−5872.
(28) Ip, A. H.; Labelle, A. J.; Sargent, E. H. Efficient, Air-Stable Colloidal Quantum Dot Solar Cells Encapsulated Using Atomic Layer Deposition of a Nanolaminate Barrier. *Appl. Phys. Lett.* **2013**, *103*, 263905.
(29) Hines, M. A.; Scholes, G. D. Colloidal PbS Nanocrystals with Size-Tunable Near-Infrared Emission: Observation of Post-Synthesis Self-Narrowing of the Particle Size Distribution. *Adv. Mater.* **2003**, *15*, 1844−1849.
(30) Burgelman, M.; Decock, K.; Khelifi, S.; Abass, A. Advanced Electrical Simulation of Thin Film Solar Cells. *Thin Solid Films* **2013**, *535*, 296−301.

DOI: 10.1021/acsenergylett.6b00314
ACS Energy Lett. 2016, 1, 740−746